Supporting Information

Photothermoelectric Response of $Ti_3C_2T_X$ MXene Confined Ion Channels

Seunghyun Hong[1,2], Guodong Zou[1], Hyunho Kim[1], Dazhen Huang[1],

Peng Wang[2,3*], and Husam N. Alshareef [1*]

1 Materials Science and Engineering, Physical Sciences and Engineering Division, King Abdullah University of Science and Technology, Thuwal 23955-6900, Saudi Arabia

2 Water Desalination and Reuse Center, Division of Biological and Environmental Science and Engineering, King Abdullah University of Science and Technology, Thuwal 23955-6900, Saudi Arabia

3 Department of Civil and Environmental Engineering, The Hong Kong Polytechnic University, Hung Hom, Kowloon, Hong Kong

* Correspondence and requests for materials should be addressed to Profs. Peng Wang (Email: peng.wang@kaust.edu.sa) and Husam N. Alshareef (Email: husam.alshareef@kaust.edu.sa)

Table of Contents

1. Morphologies of the exfoliated $Ti_3C_2T_x$ MXene sheets

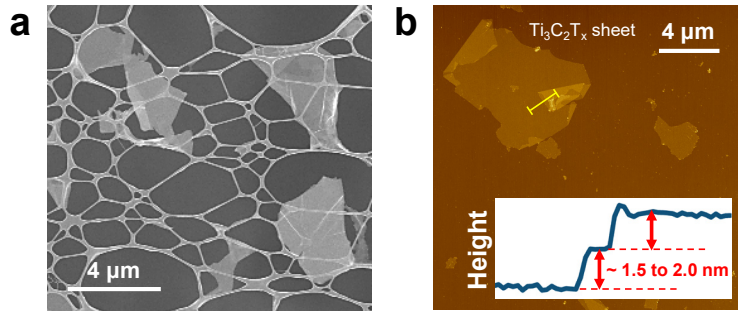

Figure S1 (a) Scanning electron microscopic image of exfoliated $Ti_3C_2T_x$ sheets deposited on holey carbon film. **(b)** Atomic force microscopic image of individual $Ti_3C_2T_x$ sheets deposited on Si/SiO_2 substrate. To avoid the effects such as instrumental artifacts or influences of contaminants on the substrate, a topographic scanning is performed on an overlapped region.[1]

2. Determination of nanochannel dimensions in lamellar MXene membranes

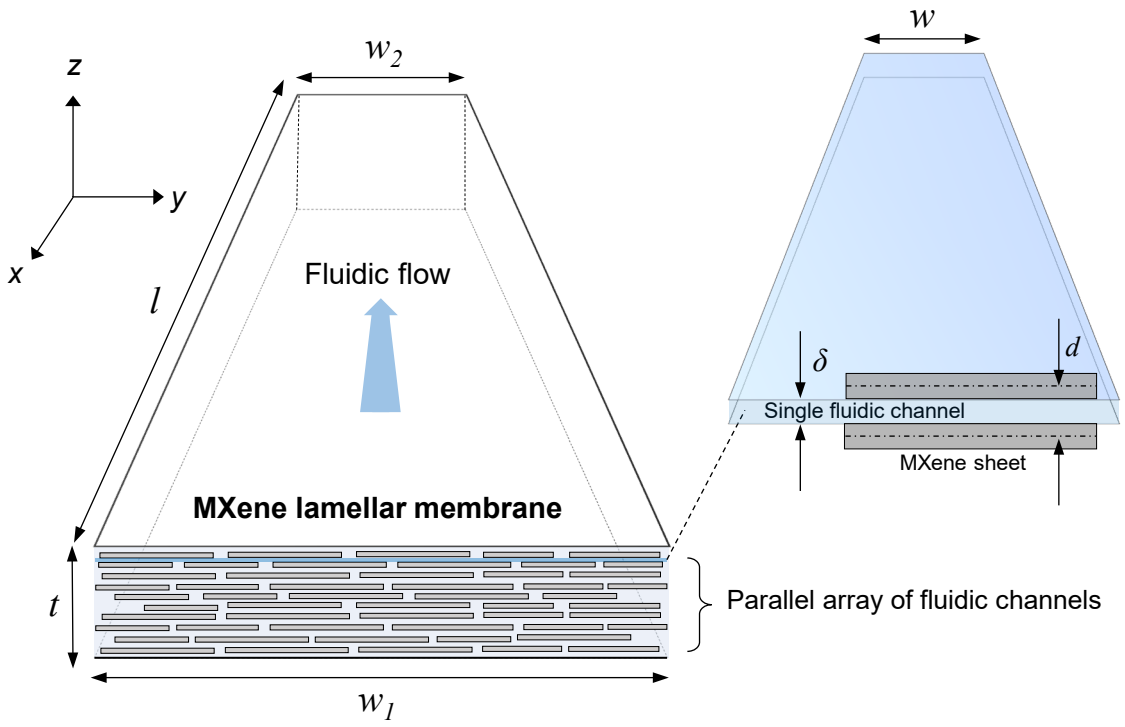

Figure S2 Geometric analysis of laminar fluidic nanochannels in the MXene membranes. The directional fluidic transport is presumed to present along *x*-axial direction, associated with thermo-osmotic cation flux under temperature-driven chemical potentials.

The MXene sheets in the multilayered membrane are separated by an interlayer distance (d) ~ 1.67 nm in fully hydrated state, as identified from XRD analysis. Given that a theoretical thickness (a) of monolayer $Ti_3C_2T_x$ sheet is ~ 0.98 nm, the effective interplanar spacing for ion transport, corresponding to the height of a nanochannel, is estimated to $\delta = (d - a)$ ~ 0.69 nm. In fully-hydrated MXene lamellar membrane, the molecular/ionic transport is assumed to present in a parallel array of a simplified two-dimensional fluidic channel having the width ($w = w_1 = w_2$), height (δ), and length (l). Here, the width, height, and length of the single channel are approximately 3 mm, 0.69 nm, and 10 mm, respectively. The total number (n) of parallel two-dimensional fluidic channels can be estimated as by ~ t/d at ambient condition, and a resulting number of channels is around 1570 across the cross-sectional area of the employed 2 μm-thick membrane at ambient. Taking into account a volumetric expansion of the MXene lamellar membrane in hydration, the effective permeation area and total membrane area are 3.27×10^{-9} m^2 and 7.85×10^{-9} m^2, respectively, which yields effective pore fraction of approximately 41.7 %. Even though the lamellar membranes are embedded in the PDMS matrix, the hydration-induced interlayer expansion is presumed to work as previously reported. [2-6]

3. Photothermal response of the MXene cation channels

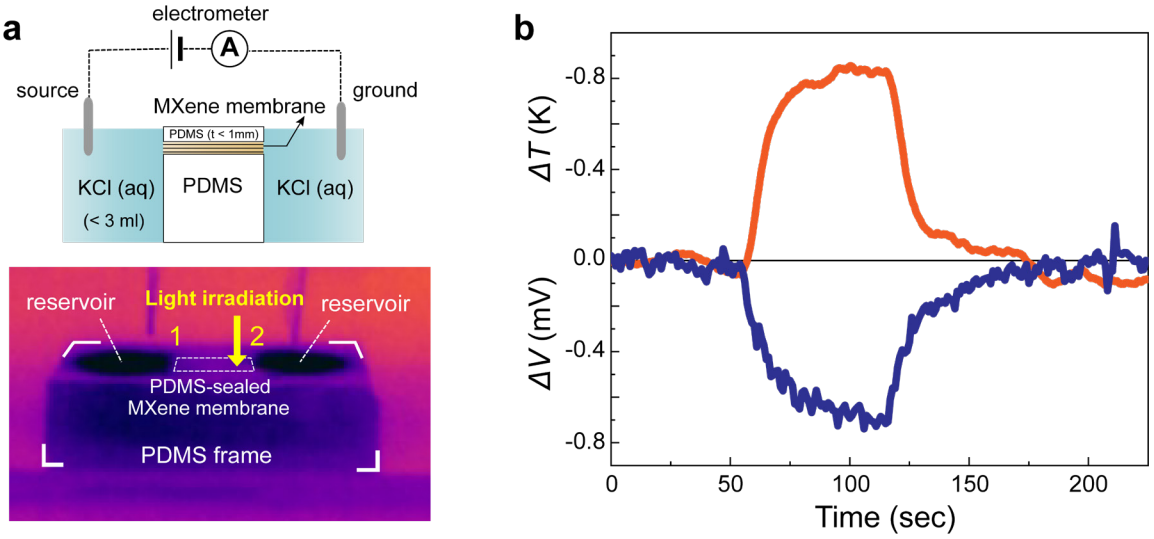

Figure S3 (a) Schematic of experimental setup. Infrared image of the PDMS-sealed MXene fluidic cell is captured by a thermographic camera under light illumination. **(b)** Synchronized thermal voltage and temperature gradient under light illumination of 127 $mW \cdot cm^{-2}$. The response speed, defined by $t_T/t_{V_{OC}}$ where $t_{V_{OC}}$ is time spent on the increase of open-circuit voltage from initial value to maximum and t_T is time spent on the corresponding temperature change, is estimated to be close to approximately 1.0.

4. Effect of prolonged light irradiation on the photothermal voltage generation

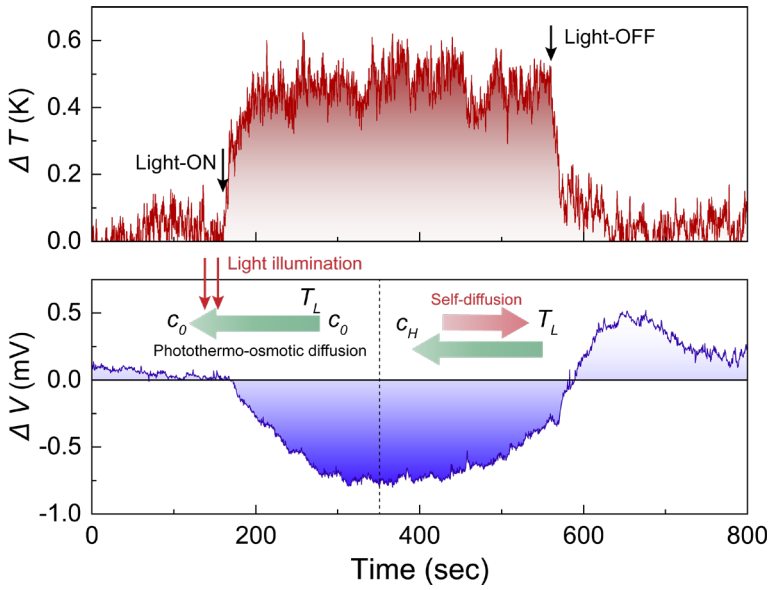

Figure S4 Under light illumination of intensity 74 mW·cm^{-2}, the temperature gradient along the cation channels is stabilized after light exposure for 60 sec and sustained till the end of the light illumination. Even under stable temperature gradient, the photothermal voltage after long-term light exposure over 3 min gets gradually decreased, followed by overturn after lights out. The observed reverse transport is possibly due to the ionic diffusion under salt concentration gradient derived from the photothermal ion flux.

5. Nb_2CT_X MXene-guided ion channels

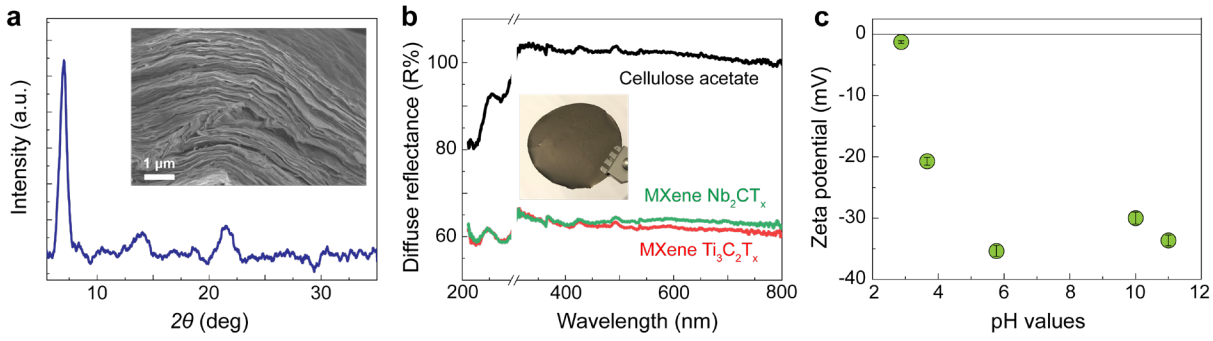

Figure S5 (a) X-ray diffraction of the hydrated Nb_2CT_x lamellar membranes. A SEM image in the inset shows the cross-sectional area of the MXene membrane **(b)** Diffusion reflectance of the membranes. Inset shows the optical image of the Nb_2CT_x membrane. **(c)** Zeta potentials of aqueous Nb_2CT_x suspension at different pH conditions. The pH-dependent zeta potentials confirm existing negative-charged functionalities and its strong protonation at lower pH conditions. The isoelectric pH near pH 3 supports the negative surface polarity of sheets at hydrated state.

6. Solid-state thermoelectric transport of $Ti_3C_2T_x$ and Nb_2CT_x MXene membranes

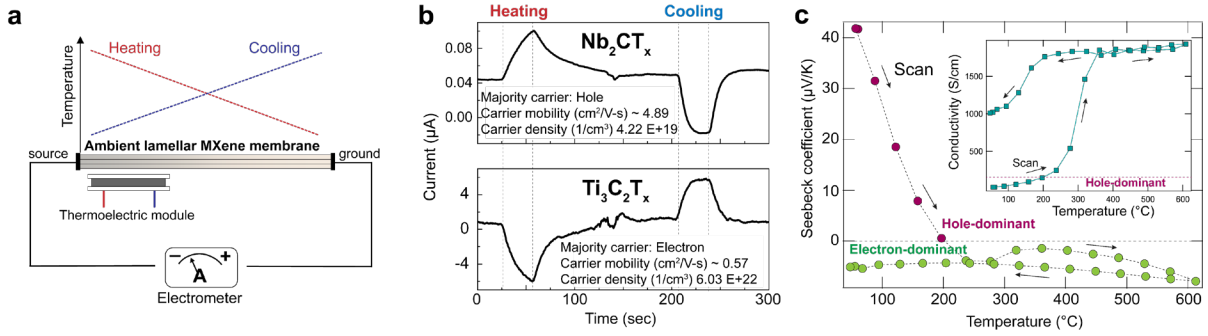

Figure S6 (a-b) Static thermoelectric carrier transport. $Ti_3C_2T_x$ and Nb_2CT_x show, respectively, opposite directionality in thermoelectric transport under thermal gradient. Inset describes data collected from Hall effect measurement for $Ti_3C_2T_x$ and Nb_2CT_x, respectively. **(c)** Seebeck coefficient measurement of the Nb_2CT_x lamellar film. The *p*-type transportation features governed by hole carriers were revealed in a temperature range of interest (initial temperature below 200 °C).

7. Photothermal response of Nb_2CT_X MXene membranes

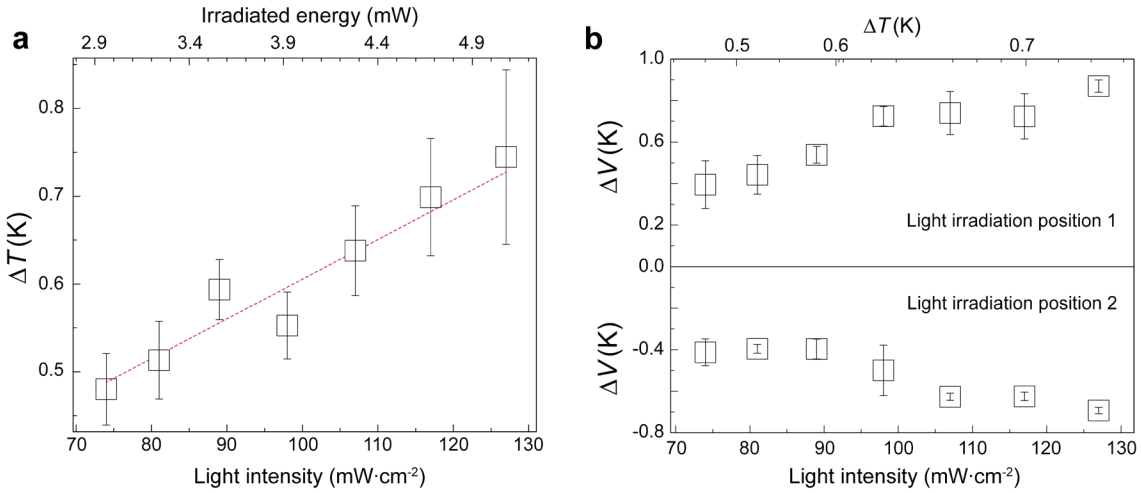

Figure S7 (a) Temperature gradient under varying light intensity. The KCl concentration is fixed to 5×10^{-4} mol·L^{-1}. The Nb_2CT_x conduits exhibited a photothermal conversion performance at the rate of 0.12 K·mW^{-1} **(b)** Photothermal voltages under elevated light intensity at different irradiation positions. The Nb_2CT_x MXene channels exhibit the ionic Seebeck coefficient of up to ~ 0.9 mV·K^{-1}.

8. Ionic transport under Joule heating-driven temperature gradient

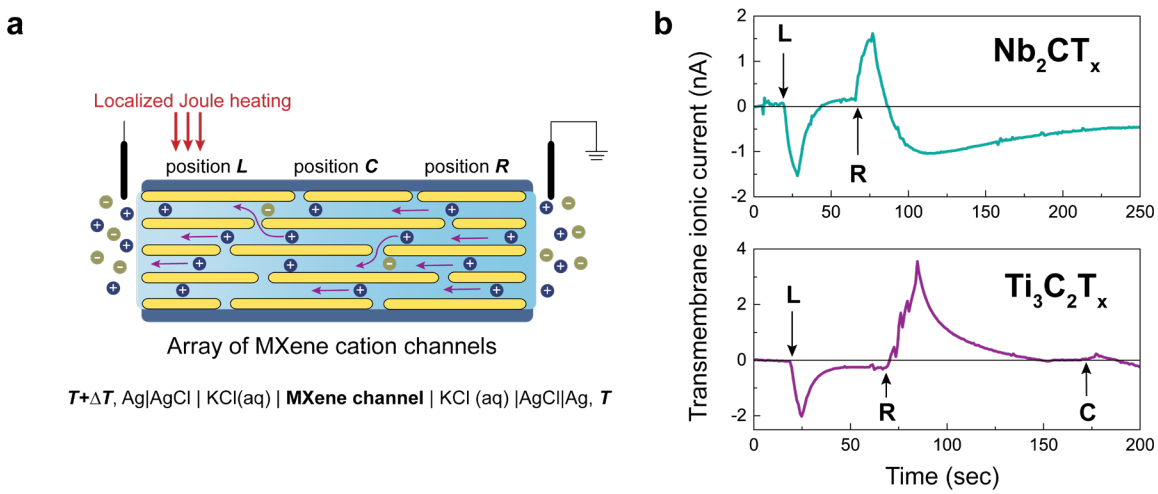

Figure S8 (a) Schematic of experimental setup. Carbon nanotube–polyvinyl alcohol composite films (3.5 × 3.5 mm^2) were applied as a Joule heater electrically connected with a DC power supply. **(b)** Localized Joule heating-driven thermo-osmotic transport. Both of MXene membranes, Nb_2CT_x and $Ti_3C_2T_x$, display consistent thermal ionic current in response to direct heating. When the thermal contact was applied to the central part, the electric potential distribution is symmetric and balanced between the two ends, showing negligibly small response.

9. Comparative study with commercially available cation exchange membranes

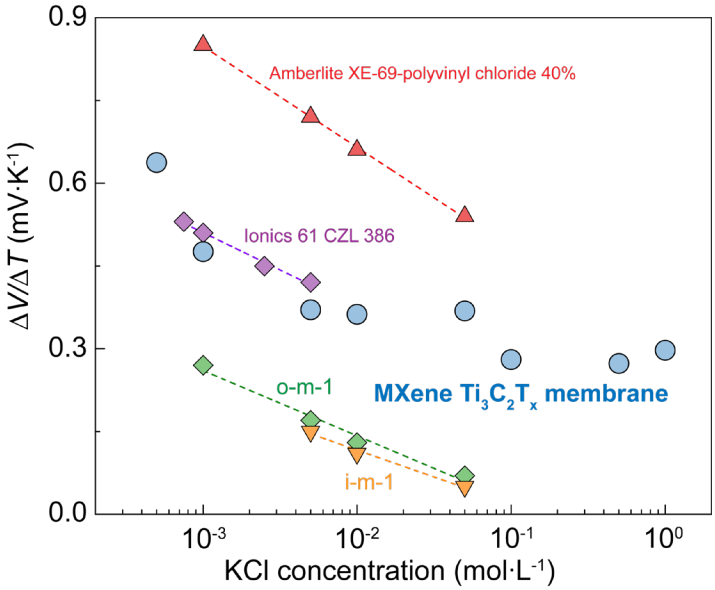

Figure S9 KCl concentration-dependent ionic Seebeck coefficient of $Ti_3C_2T_x$ MXene lamellar membranes in comparison with those from commercially available cation exchange membranes. [7-11]

10. Photothermal voltage generation at lower pH

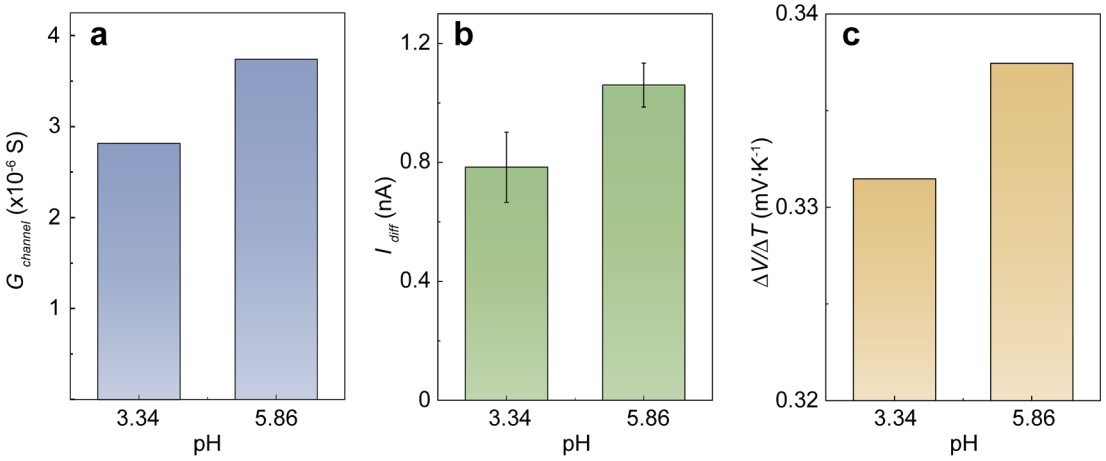

Figure S10 (a) Ionic conductance and **(b-c)** Photothermal ionic current and voltage under light illumination. The photothermal ionic transport was measured at different pH under local light illumination with the intensity of 100 mW·cm^{-2}. The KCl concentration is fixed to 10^{-2} mol·L^{-1}, and the pH condition is adjusted with hydrochloric acid. The ionic contribution from the excess hydronium at lower pH was subtracted according to previously reported protocol.[12, 13]

11. Photothermo-sensation device

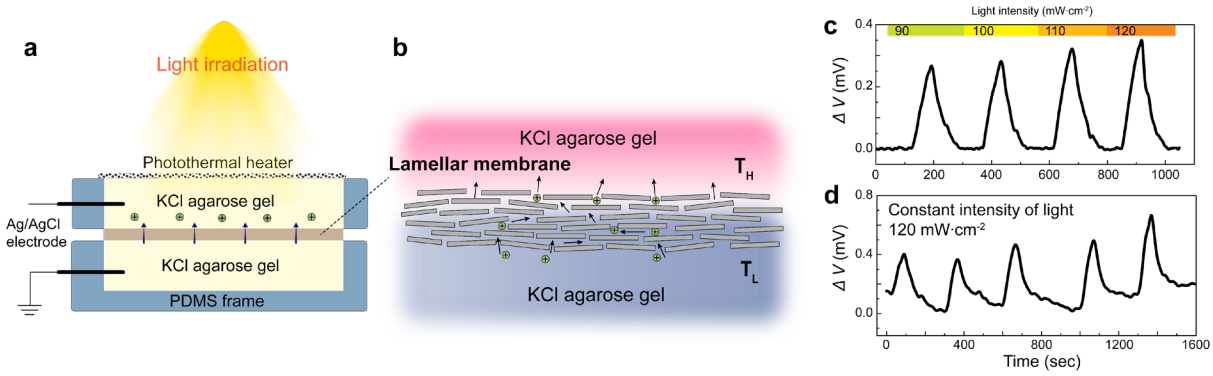

Figure S11 (a-b) $Ti_3C_2T_x$ MXene lamellar membranes (ϕ 10 mm) in contact to agarose-stabilized KCl-gel wherein stable thermal conduction can be achieved under photothermal heating. Here the agarose gel with KCl 10^{-3} mol·L^{-1} was applied, and carbon nanotube–polyvinyl alcohol composite films with ultrahigh optical absorptivity was utilized as a photothermal heater under light illumination.[14] Due to small temperature change under light, the derived variation of redox potential is presumed to be negligible. **(c)** Thermoelectric voltage generation under light with elevated intensity **(d)** Stable thermoelectric voltage in response to constant temperature gradient.

Supporting references

1. Solís-Fernández, P.; Paredes, J. I.; Villar-Rodil, S.; Martínez-Alonso, A.; Tascón, J. M. D. Determining the Thickness of Chemically Modified Graphenes by Scanning Probe Microscopy. *Carbon* **2010**, *48*, 2657-2660.
2. Raidongia, K.; Huang, J. Nanofluidic Ion Transport through Reconstructed Layered Materials. *J. Am. Chem. Soc.* **2012**, *134*, 16528-16531.
3. Shao, J.-J.; Raidongia, K.; Koltonow, A. R.; Huang, J. Self-Assembled Two-Dimensional Nanofluidic Proton Channels with High Thermal Stability. *Nat. Commun.* **2015**, *6*, 7602.
4. Qin, S.; Liu, D.; Wang, G.; Portehault, D.; Garvey, C. J.; Gogotsi, Y.; Lei, W.; Chen, Y. High and Stable Ionic Conductivity in 2D Nanofluidic Ion Channels between Boron Nitride Layers. *J. Am. Chem. Soc.* **2017**, *139*, 6314-6320.
5. Gogoi, R. K.; Neog, A. B.; Konch, T. J.; Sarmah, N.; Raidongia, K. A Two-Dimensional Ion-Pump of a Vanadium Pentoxide Nanofluidic Membrane. *J. Mater. Chem. A* **2019**, *7*, 10552-10560.
6. Yang, J.; Hu, X.; Kong, X.; Jia, P.; Ji, D.; Quan, D.; Wang, L.; Wen, Q.; Lu, D.; Wu, J.; Jiang, L.; Guo, W. Photo-Induced Ultrafast Active Ion Transport Through Graphene Oxide Membranes. *Nat. Commun.* **2019**, *10*, 1171.
7. Barragán, V. M.; Kristiansen, K. R.; Kjelstrup, S. Perspectives on Thermoelectric Energy Conversion in Ion-Exchange Membranes. *Entropy* **2018**, *20*, 905.
8. Tasaka, M.; Nagasawa, M. Nonisothermal Membrane Phenomena through Charged Membranes. *J. Polym. Sci. Polym. Symp.* **1975**, *49*, 31-42.
9. Tasaka, M.; Hanaoka, K.; Kurosawa, Y.; Wada, C. Thermal Membrane Potential through Charged Membranes in Electrolyte Solutions. *Biophys. Chem.* **1975**, *3*, 331-337.
10. Tasaka, M.; Abe, S.; Sugiura, S.; Nagasawa, M. Thermoosmosis through Charged Membranes. *Biophys. Chem.* **1977**, *6*, 271-278.
11. Barragán, V. M.; Ruiz-Bauzá, C. Effect of Unstirred Solution Layers on the Thermal Membrane Potential through Cation-Exchange Membranes. *J. Membrane Sci.* **1997**, *125*, 219-229.
12. Hong, S.; Constans, C.; Surmani Martins, M. V.; Seow, Y. C.; Guevara Carrió, J. A.; Garaj, S. Scalable Graphene-Based Membranes for Ionic Sieving with Ultrahigh Charge Selectivity. *Nano Lett.* **2017**, *17*, 728-732.
13. Hong, S.; Ming, F.; Shi, Y.; Li, R.; Kim, I. S.; Tang, C. Y.; Alshareef, H. N.; Wang, P. Two-Dimensional $Ti_3C_2T_x$ MXene Membranes as Nanofluidic Osmotic Power Generators. *ACS Nano* **2019**, *13*, 8917-8925.
14. Dongare, P. D.; Alabastri, A.; Pedersen, S.; Zodrow, K. R.; Hogan, N. J.; Neumann, O.; Wu, J.; Wang, T.; Deshmukh, A.; Elimelech, M.; Li, Q.; Nordlander, P.; Halas, N. J. Nanophotonics-Enabled Solar Membrane Distillation for Off-Grid Water Purification. *Proc. Natl. Acad. Sci.* **2017**, *114*, 6936-6941.